объединенный
институт
ядерных
исследований
дубна

E7-85-575

M.Biedermann*, P.Mädler

A TWO-STAGE MODEL FOR FAST PARTICLE EMISSION IN HEAVY-ION COLLISIONS

Submitted to "Zeitschrift für Physik A"

* Technische Universität Dresden,
Sektion Physik, 8027 Dresden, DDR

1985

Бидерманн М., Медлер П. E7-85-575

Двухстадийная модель испускания быстрых частиц в столкновениях тяжелых ионов

Используя траекторную модель Берча, мы комбинируем два физически различных подхода к описанию испускания быстрых частиц. В ранней стадии мы рассчитываем испускание частиц в духе механизма фермиевских струй. В последующей стадии, после образования шейки, предполагается испускание из быстро расширяющейся горячей зоны относительно большого начального размера, которая сильно анизотропна в импульсном пространстве. Рассчитаны дважды-дифференциальные сечения для испускания предравновесных нейтронов. Не вводя свободных параметров, мы получаем замечательное совпадение с экспериментом.

Работа выполнена в Лаборатории теоретической физики ОИЯИ.

Препринт Объединенного института ядерных исследований. Дубна 1985

Biedermann M., Mädler P. E7-85-575

A Two-Stage Model for Fast Particle Emission in Heavy-Ion Collisions

Using Bertsch's TDHF-motivated trajectory model we combine two physically distinct approaches to describe fast particle emission. In the early stage we calculate particle emission in the spirit of the Fermi-jet mechanism. In the later stage, after neck formation, particles are assumed to be emitted from a rapidly expanding hot zone of appreciably large initial dimension, which is strongly anisotropic in momentum space. We calculate absolute double-differential cross sections for preequilibrium neutron emission and obtain a remarkable agreement with experimental data without introducing free parameters.

The investigation has been performed at the Laboratory of Theoretical Physics, JINR.

Preprint of the Joint Institute for Nuclear Research. Dubna 1985

1. Introduction and Motivation

In recent years extensive experimental investigations have been devoted to the emission of nonevaporative fast particles from heavy-ion reactions at incident energies well above the Coulomb barrier (cf., e.g./1/ and references cited therein). A variety of theoretical models based on very different physical assumptions have been developed and more or less successfully applied to analyze (mostly inclusive) experimental data. If restricting consideration to fast nucleon emission only, these models can be classified according to their assumptions on the role of two-body nucleon-nucleon collisions. In the rotating hot spot model/2-4/, two-body collisions are implicitly assumed to dominate the reaction, i.e. to produce a short mean free path (MFP) and a short relaxation time leading to the formation of a static, locally excited region that statistical emitts particles. In precompound (exciton) models /5-9/, the equilibration process which is governed by two-body collisions is explicitly followed in time with a certain probability for emission from each of the intermediate states. Direct knockout models/10/ assume a single two--body collision to be the source of nonequilibrium nucleons. In the models of prompt emitted particles (PEP)/11-15/ the role of the collisions is implicitely assumed to be the source of the mean field in which the nucleons move quasifreely. The treatment of particle emission in the framework of dissipative diabatic dynamics/16/, in the mean-field model of/17/ as well as in the fully self-consistent time-dependent Hartree-Fock approximation (TDHF) /18,19/ in certain respects can be considered as quantum mechanical analogues of the classical PEP-model.

Any of the mean-field models yields angular distributions of the fast particles which are stronger peaked about the beam direction than one observes in experiment (cf./17,20/). Moreover, for symmetric systems they would predict a pronounced forward-backward peaking of the c.m. angular distributions due to the large transparency inherent in these models. This prediction is in disagreement with recent experimental data on light symmetric (or nearly symmetric) systems like $^{12}C + ^{12}C$, $^{16}O + ^{12}C$ which exhibit nearly isotropic angular distributions at energies from 85 MeV/A down to at least 25 MeV/A [21-23]. On the other hand, moving-source "models" that effectively (if understood literally) are close to the opposite extrem (hot spot, or fireball picture), work well in a wide range of incident energies and projectile-target combinations [1,20]. If extreme forward angles are excluded, the fitted values of source temperatures are smoothly increasing functions with energy, whereas the source velocities are close to half the beam velocity above the Coulomb barrier. Somewhat enhanced cross sections at very forward angles indicate the presence of direct (or prompt) emission at the very early stage of the collision and can approximately be described by PEP-models or a more involved direct reaction theory.

It is intriguing that even more exclusive experiments on fast particle emission can be quantitatively understood by taking into account translational as well as rotational motion of a statistically emitting source and - for light systems - recoil effects[23,24].

To a large extent the statistical character of the above experimental findings is, of course, connected with an experimental averaging over a huge number of microscopic channels. This seems to allow one to use theoretical concepts containing statistical elements from the outset instead of trying to develope an appropriate microscopic scattering theory and to average over the final results in order to compare with experiments. The problem is to clear up the interplay between mean-field dynamics and residual interactions without ad hoc assumptions. Corresponding information can be extracted from very recent numerical solutions of the Vlasov-Uehling-Uhlenbeck (VUU) equation in three spatial dimensions [25-28] as well as from a series of one-dimensional studies of slab collisions in TDHF including a collision term (ETDHF) [29-32]:

i) Part of the nucleons escape without having had a collision (PEP, and slipped-through projectile- or target-like fragments in the case of light systems). Its number exponentially decreases with increasing target diameter. An upper limit of the MFP of 2.6 fm at 85 MeV/A has been deduced [28].

ii) Most of the particles are emitted from a mid-rapidity system (formed with mostly multiple-scattered nucleons) that shows almost isotropic emission pattern [28].

iii) Unfortunately, the formation of that source has not been studied in detail in[25-28]. However, a mean collision number per nucleon of about twenty in the first roughly 10^{-22}s in such a small system like ^{16}O + ^{12}C at 25 MeV/A has been quoted /27/. Hence, the mean collision time appears to be much smaller than 10^{-22}s. For the same system it has been established that particles are emitted from the overlap region as well as from the other parts of the nuclei /27/. This means that the emitting "source" should have an effective spatial extent not smaller than the dimension of such a light system.

iv) Additional information on the early stage of the collision can be extracted from /29/: Shortly after contact a slight compression occurs in the overlap zone. The density "front" remains relatively stable in shape and moves with about sound velocity /33/ towards the outer ends of the slabs. The compressed region is thermalized, and in a good lowest-order approximation one can speak about a temperature front which coincides with the density front (cf. Fig. 6 of /29/ up to $t = 2\cdot 10^{-22}$s). Although this rapidly expanding "hot zone" (HZ) is characterized by a temperature field, it is far from overall statistical equilibrium since the internal parallel pressure (along the collision axis) substantially exceeds the pressure in transverse directions. When the HZ has extended over the whole volume both pressure components come close together. One could argue that these properties are simply caused by the relaxation-time approximation for the collision term used in /29/. However, in a recent paper /32/ this point has been investigated and a reasonable agreement with a more involved treatment of the collisions /34/ could be established.

In the present paper we propose a phenomenological model for the description of fast nucleon emission which combines two basically distinct mechanisms. The underlying physical picture is motivated by the above statements. At the early stage of the reaction, when the nuclei have only a small spatial overlap and the nucleonic momentum distribution is still close to two overlapping Fermi-spheres, we calculate particle emission in the framework of a certain modification of the classical PEP-model. At the later stage, after neck formation and disappearance of the single-particle potential barrier between the nuclei, we consider emission from a rapidly expanding, hot, and highly anisotropic zone of appreciably large initial dimension that does not contradict with MFP arguments. The basic differences of our HZ-picture from that of /35/ are:

i) We account for a coordinate- and time-dependent mean-velocity field in the local Fermi distribution function of the HZ. As a consequence, for asymmetric systems, we get forward-peaked angular distributions in the c.m. system (instead of backward-peaked as in /35/) which are nearly isotropic in a system moving with half the beam velocity above the Coulomb barrier. For symmetric systems we get nearly isotropic angular distributions, even at incident energies as small as 10 MeV/A.

ii) We fix the initial radius of the HZ from MFP-arguments, and from recent results of proton-proton correlation measurements at small relative angles. The value we shall use throughout this paper (3.6 fm) is even larger than the sharp-surface radius of the compound nucleus ^{24}Mg formed, e.g. in a ^{12}C + ^{12}C collision (3.32 fm).

iii) In the sense of a lowest-order approximation to the ETDHF-results described above we postulate a temperature front moving with sound velocity outwards and, to some extent, neglect heat diffusion between the HZ and the could zone (CZ). In this picture the relaxation time τ for the colliding system is given by the time which the front needs to reach the outer end of the larger interaction partner.

iv) At least at the first (PEP) stage we treat the friction force and particle emission in a consistent way starting from the nucleon flux between the ions.

The paper is organized as follows: In Sects. 2,3, and 4 we describe the trajectory model, the PEP-model, and the HZ-model, respectively. Sect. 5 deals with a comparison with experimental data and a discussion of incident-energy and projectile-mass-number dependences of fast neutron emissinn.

In a subsequent paper /36/ we test our model against recent correlational measurements.

2. Dynamics of the Collision

The relative motion of the colliding ions is followed within a classical collision model /37/ which reflects the bulk dynamics of realistic TDHF calculations.

The geometry of the model is that of three touching circles representing the two nuclei and a joining neck (Fig. 1). Only two of the three collective variables r, r_{neck}, and c are independent due to a simple geometrical relation between them and the nuclear sharp-surface radii $R_i = 1.15\cdot A_i^{1/3}$. The neck evolution is given by

$$\dot{c} = \alpha / c \qquad (1)$$

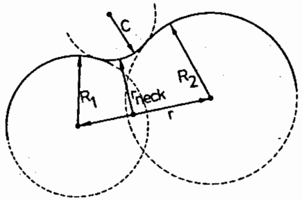

Fig. 1. Geometry of the Bertsch model

in the approach phase, and

$$\dot{r}_{neck} = -\beta\, \dot{r}_L \qquad (2)$$

in the rebound phase of the collision. Here $\dot{r}_L$ denotes the longitudinal component of the relative velocity of the two mass centers. The classical equation of motion for the relative coordinate $\vec{r}$ contains Coulomb, bulk, and surface forces. Some deviation of the Coulomb force from that of two point charges is taken into account in the rebound phase (two spheres plus a joining cylinder). The surface force is written as

$$\vec{F}_s = 2\pi\sigma \frac{\vec{r}}{r} r_{neck} \qquad (3)$$

with σ being the surface tension. Before neck formation, instead of $\vec{F}_s$, the Bass force is included. The bulk force is determined by the window formula

$$\dot{n} = \frac{3}{16} \rho_0 v_F \pi r_{neck}^2 \qquad (4)$$

describing the one-sided particle flux through the window area in the Fermi gas model ($\rho_0 = 0.16$ fm^{-3}, $v_F = 0.28c$). Before neck formation the static parametrization of [38] for the tunneling flux is used instead of (4). Memory effects are approximately included by retarding the time argument of the radial velocity entering the bulk force. In accordance with TDHF calculations neck formation is assumed to occur 9 fm/c after the potential radii (1.25 $A_1^{1/3}$) touch. We adopt the standard parameter set of [37]: α = 0.04 fm/c, β = 1/3, σ = 1 MeV fm^{-2}. Details of the model and extensive comparisons with experimental data as well as with TDHF results can be found in [37,39].

In the present paper we use a slightly modified version [39] of the model. While in the original version [37] the particle flux between the ions has a discontinuity at the instant at which the neck opens (due to different expressions used for $\dot{n}$ before and after), we formally enforce continuity by using the maximum value of the tunnel flux, reached before switching over to (4), until (4) yields a larger value. In any case this modification concerns only a very small time interval. It prevents, however, the friction force from being attractive for some instants during the approach phase which would happen for asymmetric systems and higher incident energies.

For a given incident energy and impact parameter, we start the numerical iteration of the equations of motion at an initial distance $r(t=0) = 1.25\,(A_1^{1/3} + A_2^{1/3}) + 4$ fm assuming a pure Coulomb trajectory for $t < 0$. We neglect any influence of particle emission on the trajectory. In [15] this has been checked to be a good approximation.

Finally we quote some trajectory results concerning the reactions investigated in this paper: For the system ^{20}Ne + ^{181}Ta, E_{lab} = 180 MeV we obtain fusion for initial angular momenta up to 72 $\hbar$, a deep inelastic behaviour from 73 $\hbar$ to 87 $\hbar$, while for $L \geq 88\,\hbar$ no neck appears (quasielastic collisions). For the ^{20}Ne + ^{165}Ho system we find a critical angular momentum for fusion of 85 $\hbar$ compared to a value of 95 $\hbar$ determined experimentally [20]. Since from the measured cross sections for evaporation residues (ER) it follows that above $L \approx 60\,\hbar$ fission occurs after fusion for all bombarding energies considered in [20], we shall use this value as the upper limit in the L-integration when comparing our model predictions with the data on fast neutrons in coincidence with ER.

3. The PEP-Model

Since PEP-models have been extensively described in the literature [11-15] we concentrate on the specific features of our version only. The cross section for PEP emission is given by [11]

$$\sigma = 2\pi \int b\, db \int dt \int d\vec{A} \int d\vec{v}_a\, f(\vec{v}_a)\, \vec{j}_A(\vec{v}_b)\, e^{-d/\lambda} . \qquad (5)$$

Integration over time t , impact parameter b , window area A, and velocity $\vec{v}_a$ of the nucleons in the donor nucleus are involved. The velocity of a nucleon with $\vec{v}_a$ in the donor is $\vec{v}_b = \vec{v}_a + \dot{\vec{r}}$ in the recipient. The velocity distribution function f is taken to be a zero-temperature Fermi distribution. The exponential factor in (5) describes absorbtion with d being the distance traversed by the prospective PEP inside the recipient, and λ being the nucleon MFP. We calculate λ from the imaginary part of the optical nucleon-nucleus potential like in /11,14,15/. Also the usual escape conditions are applied.

Opposite to other PEP-models we calculate the local one-sided flux $\vec{j}_A(\vec{v}_b)$ through a given surface element $d\vec{A}$ in a way, more consistent with the evaluation of the friction force. We achieve this by requiring its normalization to the total flux $\dot{n}$ (tunnel flux or eq.(4) before and after neck formation, respectively) at each instant:

$$\int d\vec{A} \int d\vec{v}_a \; f(\vec{v}_a)\,\vec{j}_A(\vec{v}_b) = \dot{n} . \qquad (6)$$

Except the time-dependent normalization constant defined by (6), the velocity spectrum of $\vec{j}_A$ is given by the product $\vec{v}_b P$ where P stands for the tunnelling probability of a nucleon through the single-particle barrier between the nuclei.

After neck formation, when the barrier is assumed to vanish, we put $P \equiv 1$. The window area over which integration in (5), (6) has to be performed simply coincides with the neck area πr^2_{neck} in this case. Although we allow the nucleons to emanate from any point of the window, we do not consider sidewards emission directly through the neck (circle of radius c in Fig. 1) as it has been done in /15/. Due to the small transverse spatial extent of the neck, it seems to us that with this respect the assumption of an unperturbed Fermi distributinn is questionable (even at the early stage of the collision). Moreover, such particles are not seen in self-consistent mean-field theories.

Before neck formation we use an approximate analytical expression for P obtained in the following way: We assume the barrier to be the sum of two Woods-Saxon potentials centered at relative distance r and characterized by the half-density radii $\tilde{R}_i = R_i - b^2/R_i$ (R_i - sharp-surface radii), the diffuseness parameter b = 0.7 fm, and a depth of V_0 = -45 MeV. Then, for nucleons tunnelling along the axis joining the centers of the nuclei, we have to calculate the probability $P(v,s)$ with $s = r - \tilde{R}_1 - \tilde{R}_2$ and v being the velocity of the incoming nucleon relative to the barrier. Using the Hill-Wheeler formula for a parabolic fit to the assumed barrier we get

$$P(v,s) = \frac{1}{[1 + \exp\{2\pi(\overline{V}_0 - \frac{m}{2}v^2)/\omega\}]} \qquad (7)$$

with

$$\overline{V}_0 = |V_0| \tanh(s/4b) ,$$

$$\omega = \sqrt{\tfrac{2}{m}|V_0|\tanh(s/4b)}\,/\,[2b\cosh(s/4b)] .$$

In (7), for nucleons which do not move along the symmetry axis, we use the actual distance $\tilde{s} > s$ which they traverse between the spheres of radii $\tilde{R}_i$ but do not account for the corresponding effective increase in the diffuseness. Furthermore, we put $v = |\vec{v}_a + \frac{1}{2}\dot{\vec{r}}|$ since the barrier moves with approximately half the relative velocity $\dot{\vec{r}}$ towards the donor nucleus. Hence,

$$\vec{j}_A(\vec{v}_b) \sim \vec{v}_b \, P(|\vec{v}_a + \tfrac{1}{2}\dot{\vec{r}}|, \tilde{s}_A) , \qquad (8)$$

where the index A indicates that for a given s the distance $\tilde{s}$ depends on the surface element $d\vec{A}$ from which the particle emanates. Of course, $\tilde{s}_A$ also depends on the direction of $\vec{v}_a + \frac{1}{2}\dot{\vec{r}}$. The surface area for integration in (5), (6) is assumed to be perpendicular to the axis joining the mass centers and tangential to the sharp surface of the donor nucleus. As in /11/ we assume that it linearly increase from zero at $t = 0$ to the area of the neck when it just opens. Note that this value is nonzero /37,39/. Due to the normalization (6) our results are not sensitive to other possible definitions of the window area at the early stage.

In all calculations presented below we account for both projectile- and target-like PEP.

The (time-dependent) transformation of the differential probability of emitted particles in the instantaneous rest system of the recipient to the laboratory (c.m.) system is performed by using the approximate expression for the Jacobian which has been derived in /14/ for the velocities being bracketed by discrete bins.

Since we deal in this paper only with neutron emission, the cross section for projectile- and target-like PEP are reduced by the neutron-to-mass-number ratio N/A of the corresponding donor nucleus. We neglect isospin corrections/14/ for the corresponding Fermi velocities v_F and use v_F =0.28c.

We conclude this section with some illustrative discussions. Fig. 2 shows the single-particle potential barrier between two colliding nuclei along the symmetry axis as a function of s . For any s the top of the barrier has been shifted to x =0. For the ^{20}Ne + ^{165}Ho system at E_{lab} = 220 MeV and zero impact the following relations are met: s =5.31 fm - situation at t =0; s =1.31 fm - the potential radii touch; s =0.47 fm - the sharp-surface radii

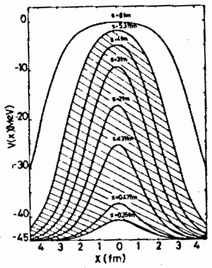

Fig. 2. Single-particle potential barrier between the colliding nuclei. For details, see text.

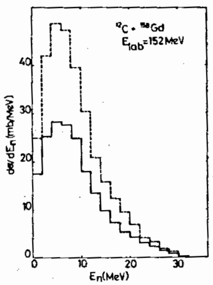

Fig. 3. Angle-integrated c.m. energy spectrum of neutron PEP's in the reaction $^{12}C + ^{158}Gd$. Full lines: present paper; dashed lines: results of /11/.

touch; $s = 0.26$ – the neck appears; $s < 0$ – the barrier is assumed to be vanished, i.e. $P \equiv 1$. The hatched region marks the situations which contribute to what we call the first (PEP-) stage of the reaction. For smaller s we apply our HZ-model as described in the next section. Only for some comparative purposes we also perform full PEP-calculations.

In Fig. 3 we compare such a calculation with the corresponding results of /11/. Our cross sections are systematically smaller by factors up to 1.7. We relate this deviation mainly to the different evaluation of the one-sided flux. The shapes of our calculated angular distributions are, however, rather close to those of /11/.

4. The Hot-Zone Model

We now describe our phenomenological HZ-model to be applied after the neck has appeared in the corresponding trajectory calculation. In quasigrazing collisions, where no neck appears, this stage is missed and only direct (PEP) emission is allowed. The aim of the model is to mimick the mid-rapidity source observed in VUU-calculations and usually described by a moving thermal source.

4.1. The initial state of the HZ

It is out of the scope of this paper to give a dynamical description of the formation of the HZ. This problem can only be attacked in more involved approaches like VUU or ETDHF. There are, however, some arguments, which together with the statements of Sect. 1 allow one to fix an appropriate initial state of the HZ:

First, we discuss trajectory results for $^{20}Ne + ^{165}Ho$, E_{lab}= 220 MeV, $L = 0\,\hbar$ with this respect. At $t = 41$ fm/c (neck opens) the energy loss due to friction is 41.5 MeV. From this energy, 69% (97%) have been dissipated during a time interval Δt as small as 9 fm/c (20 fm/c). A nucleon moving at this time from one nucleus to the other (otherwise it does not contribute to friction) with velocity v ($v \lesssim v_{max} \approx v_F + \dot{r}(t_0 - \frac{1}{2}\Delta t) \approx 0.39c, \dot{r} \approx 0.11c$) passes a distance of $\Delta x \lesssim 3.5$ fm (7.8 fm) in the neck region. Hence, classically speaking, at $t = t_0$ nucleons which have contributed to energy dissipation are inside a spatial region of diameter 7÷8 fm surrounding the neck – even if there are no two-body collisions. Since the nucleon MFP estimated in a realistic geometry for colliding ions at incident energies from 10 to about 50 MeV/A is as small as 4 ÷ 5 fm /40/, it is likely that those nucleons exhibit on the average 1 ÷ 2 collisions up to time t_0. This does not contradict the VUU-result (cf. Sect. 1) of the mean collision time being much less than 10^{-22}s (≈ 30 fm/c). Note further that the time intervals Δt are comparable to the characteristic time $\tilde{t}$ for the diffuse edges of the nuclei to pass through each other: $\tilde{t} \approx 2b/\dot{r} \approx 15$ fm/c. Hence, in the early stage ($t_0 - \Delta t \lesssim t \lesssim t_0$) two-body collisions occur mainly in the region of the overlapping surfaces, where Pauli blocking is effectively reduced due to the smaller local Fermi momenta /40/. Moreover, it may be important to note that effects not considered in /40/ could yield an additional effective decrease of the MFP: The influence of the random Fermi motion /41/ (less pronounced in N-A scattering), the "prior" Pauli effect /41/ (not present at all in N-A scattering), and other effects not connected with the short-range part of the nucleon-nucleon interaction /42/.

Since it has been found in /43,44/ that 1 ÷ 2 collisions are sufficient to bring a nucleonic system close to equilibrium, the above estimates do not contradict the assumption that at $t = t_0$ we find a nearly thermalized spatial zone of radius 3 ÷ 4 fm. At higher incident energies, similar results are obtained (smaller $\Delta t, \tilde{t}$, but larger v_{max}, hence, nearly unchanged Δx).

Second, we briefly recall some recent results concerning effective source radii extracted from proton-proton correlation measurements at small relative angles, and incident energy of 25 MeV/A /45,46/. While the observed correlations for $^{16}O + ^{12}C$, ^{27}Al can be described by a statistical calculation which incorporates the thermal emission of particle-unstable ^2He nuclei from the compound nucleus /47/, this process is suppressed in the $^{16}O + ^{197}Au$ reaction by the

Coulomb barrier and the lower temperature [46,47]. In the latter case an effective source radius of $r_0 \approx 4$ fm has been extracted [45,46]. The observed correlation function which rapidly increases with the sum energy of the protons [46] possibly indicates an increase of the source radius in time since the fastest particles are expected to be emitted in the early stage. The corresponding correlations for the ^{12}C target are nearly independent of the proton sum energy. In the ^{27}Al case the situation is similar, however, a slight increase of the correlation function at largest sum energies may indicate a link of the results for the lightest and heaviest targets considered. The value $r_0 \approx 4$ fm is larger than the radius of the compound nucleus for the lightest of those systems and, consequently, the results on p-p correlations agree with the corresponding VUU-results (cf. Sect. 1). The extracted r_0 value has to be understood as an upper limit by two reasons: A zero life time of the source has been assumed, and the measured correlations represent a time-average over the expanding source. We conclude that an initial radius of the HZ somewhat smaller than 4 fm would not contradict the experimental findings and agrees with the above estimates. Finally, we quote an argument based on estimates of the relaxation time τ for the colliding system. The simplest (but not the worst) estimate is $\tau = 2R/v_F$ (R – radius of the heavier reaction partner). On the other hand, in our model, it turns out to be the time needed by the temperature front to reach the outer surface of the heavier nucleus, i.e. $\tau = [2R - R_{HZ}(t_0)]/v_s$, v_s = 0.2c being the sound velocity. Combining both estimates we get

$$R_{HZ}(t_0) = 2R\,(1 - v_s/v_F) \qquad (9)$$

which yields 3.6 fm for ^{165}Ho and 3.7 fm for ^{181}Ta. Without taking (9) too seriously, we shall use

$$R_{HZ}(t_0) = 3.6\,fm \qquad (10)$$

throughout in this paper. We have checked that the final results (double-differential cross sections) do not drastically change if enlargening or lowering that value by 0.5 fm. Then, the largest deviations – up to a factor of 2 – appear for the highest energies of the particles emitted in forward directions. For lighter targets we would prefer to apply the model (if at all) with (10) instead of (9), since this would agree with the VUU-results concerning light systems discussed in Sect. 1, while (9) would yield too small initial HZ radii (1.5 fm for ^{12}C, 2 fm for ^{27}Al). The latter probably reflects the fact that the picture of a sharp temperature front is less applicable in the case of light nuclei.

We determine the initial excitation energies of the HZ and the cold zone (CZ) from the work that has been done by the friction force $\vec{F}_f$ along the trajectory up to $t = t_0$, and the "preheating" of the whole system $E^*_{pre}(t_0)$ due to those prospected PEP's which have been reabsorbed in the nuclei:

$$E^*_{HZ}(t_0) = -\int_{+\infty}^{\vec{r}(t_0)} \vec{F}_f(\vec{r})\,d\vec{r} - \left[1 - V_{HZ}(t_0)/V(t_0)\right] E^*_{pre}(t_0) \qquad (11)$$

$$E^*_{CZ}(t_0) = E^*_{pre}(t_0)\, V_{CZ}(t_0)/V(t_0) \qquad (12)$$

with $V_{CZ} + V_{HZ} = V$ being the total volume of the system. The corresponding temperatures $T_{HZ}(t_0)$, $T_{CZ}(t_0)$ are defined from (11), (12) using level density parameters $a_{CZ}(t_0) = A_{CZ}(t_0)/8$, and $a_{HZ}(t_0) = \pi^2 A_{HZ}(t_0)/4\,\varepsilon_F$ with a constant density ρ_0 = 0.16 fm^{-3}, and calculating the partial volumes according to the geometry of the system (see Figs. 7,9 below). Some remarks are in order: First, we neglect the density dependence of the Fermi energy ε_F as well as of the particle number A_{HZ} since we have no dynamical equation for the time-dependence of the HZ-density ρ_{HZ}. On the other hand ρ_{HZ} enters into the final results on particle emission essentially only through the ρ_{HZ} –dependence of T_{HZ}. It can easily be shown that for given V_{HZ} and E^*_{HZ} in the Fermi gas model $T_{HZ} \sim \rho_{HZ}^{-1/6}$, i.e. the density dependence of the temperature can be neglected for 10 – 30% initial compression which is seen, e.g. in TDHF calculations for incident energies of a few tens of MeV/A. Second, there is some ambiguity in the homogeneous deposition of E^*_{pre} at $t = t_0$: On the one hand, we have argued above that even the fastest nucleons cannot leave the HZ-region up to time t_0 (scattered or unscattered). On the other hand, PEP's are calculated at the early stage as if they would have been emitted or absorbed during $t < t_0$. This apparent contradiction is due to the fact that in none of the PEP-models, including ours, the time delay between passing through the window and being emitted has been taken into account. Actually, the particles leaving the prospected HZ-region unscattered are emitted at $t \gtrsim t_0$. Note, however, that the second term in (11) amounts only to a few percent of the first one and that T_{CZ} , E^*_{CZ} have no influence at all on the results on particle emission. Also the omission of PEP's in the energy balance (11),(12) can be checked to be a good approximation, since in any of the cases considered below their multiplicity is smaller than 0.25 in the first stage.

4.2. Temperature evolution of the HZ

We simplify the time evolution of the temperature field obtained in 1D-ETDHF calculations [29] by assuming a sharp temperature front expanding radially with sound velocity $v_s = 0.2c$. Compared to those results this seems to be a good lowest-order approximation which probably can be explained by the high nonlinearity of the ETDHF equations present also in any self-consistent theory. Note that, e.g., the relative stability of the compression front (until it reaches the outer surfaces) observed also in realistic TDHF calculations should be of similar origin. This is a nontrivial fact owing to the MFP usually said to be large. In any nonlinear theory the MFP is, however, not a well-defined quantity.

Without solving an equation for heat diffusion between the HZ and the CZ, we partially account for it in a simplified way: The CZ is further heated up by particles being emitted from the HZ-surface inside the nuclei and subsequently absorbed in the CZ (described like the "preheating" in the PEP-stage). Furthermore, if the HZ-radius has increased by dR_{HZ}, we subtract $(E^*_{CZ}/V_{CZ})\,dV_{CZ}$ from E^*_{CZ} and add it to E^*_{HZ}. Here $dV_{CZ} = dV_{HZ}$ stands for the corresponding decrease (increase) of the CZ (HZ) volume.

The main mechanism governing the temperature evolution of the HZ are, however, the further increase of the HZ-volume (cooling) and the further accumulation of energy due to friction (like in (11)). We also take into account the additional cooling due to neutron emission by lowering the actual excitation energy of the HZ by the particle energy above ε_F multiplied by the corresponding differential multiplicity. In the cases considered below this depletion has, however, been found to play a negligible role.

In Fig. 4 the time evolution of the excitation energies of both zones is shown for central collisions of the ^{20}Ne + ^{165}Ho system at two incident energies (220, and 402 MeV). Before neck formation ($t < t_0$ = 41 fm/c, and 27 fm/c, respectively) only the preheating excitation energy $E^*_{pre}(t)$ is shown which we deposite at $t = t_0$ according to (11),(12). Due to the rapid decrease of V_{CZ}, E^*_{CZ} rapidly decreases. The HZ-excitation energy increases further for $t > t_0$ up to the turning point followed by a slight decrease. The latter is

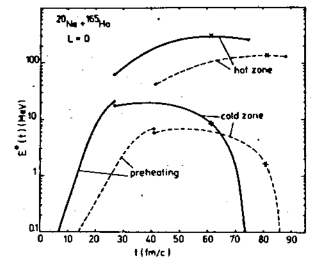

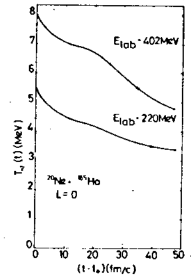

Fig. 4. Time evolution of the "preheating"-, HZ-, and CZ-excitation energies for central ^{20}Ne + ^{165}Ho reactions at 402 MeV (full lines) and 220 MeV (dashed lines) bombarding energy. Crosses and the end points of the lines mark the turning point, t_0, and τ, respectively.

Fig. 5. HZ-temperature evolution for the same system as in Fig. 4.

mainly connected with the time-retarded friction force which is still repulsive for a certain time interval after the turning point, and to a less extent with depletion due to emission.

Fig. 5 illustrates the corresponding HZ-temperature evolutions. The shoulder arround $(t - t_0)$ = 20 fm/c is a result of the interplay between expansion and energy accumulation: After the front having reached the center of the Ho nucleus the rate of change of the HZ-volume is smaller than at the early stage (cf. Fig. 7) while still a substantial dissipation takes place. Note that the initial temperatures (which mainly determine the high-energy tails of the spectra) are close to the values extracted from a moving source fit for the same reactions in [20] (4.5 ± 0.3 MeV and 8.6 ± 0.3 MeV, respectively).

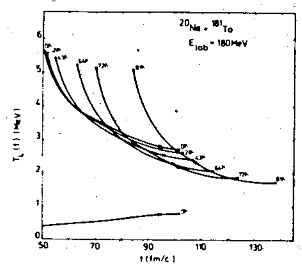

Fig. 6. Time-dependence of T_{HZ} for different initial angular momenta for the ^{20}Ne + ^{181}Ta reaction. The lowest curve represents the time evolution of T_{CZ} for a central collision.

From Fig. 6 we get some information on the impact parameter dependence of T_{HZ}. We observe that the initial temperature $T_{HZ}(t_0)$ decreases with L, and that the decrease in time is stronger in more peripheral reactions. Hence, our model predicts an effective (time-averaged) temperature for the preequilibrium stage which is larger in central collisions than in more peripheral ones. Note that t_o also depends on L, i.e. for more peripheral collisions the neck opens at a later instant. The slight increase of T_{CZ} (shown only for $L = 0\ \hbar$ since the L-dependence is rather weak) is due to further particle absorption in the CZ. Hence, E^*_{CZ} decreases somewhat slower than the CZ-volume.

4.3. The mean-velocity field

The velocity distribution of the nucleons in the colliding system is not simply a superposition of the intrinsic Fermi motion that is characterized by two temperatures T_{HZ}, and T_{CZ} with the motion of the mass centers of the nuclei as described by the classical trajectory. At any instant $t < \tau$ the mean nucleon velocity $\bar{v}(z,t)$ along the instantaneous z-axis joining the mass centers changes smoothly from projectile- to target-like velocities. To illustrate this point we show in Fig. 7 the geometry of a $^{20}Ne + ^{165}Ho$, $L = 0\ \hbar$, E_{lab}= = 220 MeV system at $t = t_o$ + 10 fm/c. For simplicity, we shall consider a cylindrical neck of radius $r_{neck}(t)$ determined from the trajectory calculation in the following. In the lower part of Fig. 7 c.m. velocities $\langle v_i \rangle$ at $t = -\infty, t_o$ of both nuclei are indicated (horizontal thin lines). The expected behaviour of $\bar{v}(z)$ as schematically shown in Fig. 7 should exhibit the following features: The two parts of the still uneffected by the collision CZ should be characterized by $\bar{v}(z)$-values close to the initial velocities of the nuclei above the Coulomb barrier.

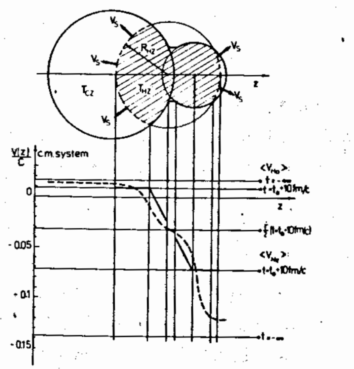

Fig. 7. The geometry of the $^{20}Ne + ^{165}Ho$, E_{lab}=220 MeV, $L = 0\ \hbar$ system at $t = t_o$ + 10 fm/c (upper part). The lower part shows the expected "realistic" (heavy dashed line) as well as the assumed (heavy full line) z-dependence of the mean-velocity field. For details, see text.

In the (compressed) HZ-region, however, it should monotonically vary between those values exhibiting a "quasistationary point" in the neck region moving with $\bar{v}(z) = \dot{r}/2$. Note that due to momentum conservation the mean velocities in the outer regions are larger in absolute value than the velocities of the mass centers $\langle v_i \rangle$ defined by the trajectory.

Since we consider particle emission only from the HZ, only some prescription for $\bar{v}(z,t)$ in that region is needed. For our first

applications we postulate:

i) $\bar{v}(z,t) = \dot{r}(t)/2$ in the neck region.

ii) Except that region, $\bar{v}(z,t)$ linearly changes between the mass-center velocities $\langle v_i \rangle$.

iii) $\bar{v}(z,t)$ becomes equal to $\langle v_i \rangle$ at the z-coordinate of the intersection between the nuclear sphere and a sphere of radius $R_{HZ}(t)$, if this point lies in the inner hemisphere of the corresponding nucleus.

iv) In the opposite case it becomes equal to $\langle v_i \rangle$ at the z-coordinate of the mass center of the corresponding nucleus.

The mean-velocity field in the HZ which would result from this prescription is also shown in Fig. 7. In the given case iii) concerns the Ho- and iv) the Ne-nucleus. The advantage of our simple dynamical definition of $\bar{v}(z,t)$ is that we have only used "fix points" which are well-defined in the model. Of course, one could try to introduce more involved parametrizations.

Next we prove to what extent our prescription may work. With this aim we have performed a series of 1D-TDHF calculations (for details, see [48]) for slab collisinns and compared the time evolution of the calculated velocity field

$$v(z,t) = \frac{1}{\rho(z,t)} \frac{\hbar}{m} \sum_n a_n \, \mathrm{Im} \left[\phi_n^*(z,t) \frac{\partial \phi_n(z,t)}{\partial z} \right] \qquad (13)$$

with our approximation. Here ϕ_n, a_n and $\rho(z,t)$ denote the single-particle wave functions, the occupation numbers ($a_n < 1$ in the slab geometry), and the single-particle density, respectively. An illustrative example is shown in Fig. 8. First we observe that the density front (DF) (defined arbitrarily as $\rho(z_{DF},t) = [\rho_o + \rho(z=0,t)]/2$ moves with $v \approx 0.25c$ which is about the velocity of thermodynamic sound in the slab geometry [33] and which should be replaced by 0.2c in three dimensions. Second, starting from the situation at t=24 fm/c ($z_{DF} \approx 4$ fm $\triangleq R_{HZ}(t_o)$) our prescription yields a good agreement with the actual values of $v(z,t)$. Here case i) does not apply since the neck region is not defined in the slab geometry. Since some over- and underestimations met at different t can partially compensate each other in the time integral for any observable quantity, we conclude that our parameter-free prescription for $\bar{v}(z,t)$ is a reasonable lowest-order approximation for the time interval $t_o \leq t \leq \tau$ of interest.

We describe the local velocity distribution of the nucleons at

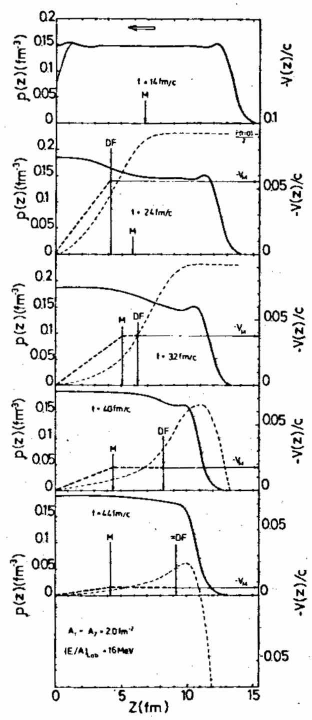

Fig. 8. Density (heavy full lines, left-hand scale) and mean-velocity field (thin dashed lines, right-hand scale) evolution in a $A_1 = A_2 = 2.0\ fm^{-2}$, $(E/A)_{Lab}$=16 MeV slab collision. Due to symmetry only half of the system is shown. The thin line at t =14 fm/c represents the unperturbed density of a static slab. The calculated mass center (M) and density front (DF) positions are indicated by vertical arrows. The thin horizontal lines denote the calculated velocities of the mass center $- v_M$. The heavy dashed lines represent the mean-velocity distribution in the compressed region according to the parameter-free prescription quoted in the text.

any point $\vec{R} = (z, \vec{R}_\perp)$ of the HZ by a generalized Fermi distribution /44/:

$$n_{HZ}(\vec{v},t,z) = \Big[1 + \exp\Big\{\Big(\frac{m}{2}\big[v^2 + \bar{v}^2(z,t)\big] - \varepsilon_F - m v \bar{v}(z,t)\cos\theta\Big)/T_{HZ}(t)\Big\}\Big]^{-1}, \qquad (14)$$

where $\vec{v}$ denotes the velocity of the nucleon considered and θ the angle between the directions of $\vec{v}$ and the mean velocity $\bar{v}(z,t)\cdot\vec{e}_z(t)$ ($\vec{e}_z$ - unit vector along the instantaneous axis joining the centers of the nuclei).

4.4. Particle emission from the HZ

The cross section for neutron emission is calculated as:

$$\sigma_{HZ} = 2\pi\int b\,db\int dt\int_{HZ} d\vec{A}\int d\vec{v}\ \ \vec{v}\,\varrho_n\, f_{HZ}(\vec{v},z,t)\, e^{-d/\lambda}, \qquad (15)$$

$$f_{HZ}(\vec{v},z,t) = \frac{3}{4\pi v_F^3}\, n_{HZ}(\vec{v},t,z), \qquad (16)$$

$$\varrho_n = \frac{(N_1 + N_2)}{(A_1 + A_2)}\,\varrho_0 . \qquad (17)$$

An integration over the whole surface of the HZ at each instant is contained in (15). The z-coordinate of the surface element $d\vec{A}$ enters into f_{HZ} . For emission from the HZ-surface region inside the nuclei the absorption factor is calculated as at the PEP-stage: for the remaining part of the surface it is simply unity. The exact normalization of (14) can only be calculated numerically at each t, z . Therefore, for simplicity, we use the approximate normalization (16). For the largest T_{HZ} and $\bar{v}(z,t)$ values appearing in the reactions considered in this paper, the corresponding errors have been checked to be <20%.

For a further simplification of the numerical expense, we consider particle emission to occur only perpendicular to the HZ-surface, i.e. we replace in (15):

$$\int d\vec{v}\,(d\vec{A}\cdot\vec{v})\ldots \longrightarrow \pi\, dA\int dv\, v^3\ldots \qquad (18)$$

The emission from the three parts of the HZ belonging to target, projectile, and neck is calculated in the corresponding instantaneous rest systems and then transformed to the laboratory (c.m.) system as described in Sect. 3.

For some qualitative discussion we return to the $^{20}Ne + ^{165}Ho$, E_{lab}= 220 MeV, $L = 0\ \hbar$ system. In Fig. 9 several calculated directions of neutrons being emitted with an energy of 11 MeV relative to the corresponding part of the nuclear surface are shown (before transformation). The dashed arrows illustrate some typical cases which we neglect according to (18). Time-integrated (from t_0 to τ) differential c.m. neutron multiplicities are shown in Fig. 10 for two different neutron energies. They exhibit pronounced, unphysical structures which can be shown to be exclusively related to our pragmatic simplifications to reduce the numerical expense, and by following the particles along classical trajectories: The peak arround $\theta_{c.m.} = 0°$ (A) is due to a strong focussing effect at the outer nuclear surfaces (cf. Fig. 9). Note that it is less pronounced for higher neutron energies. The dip near $\theta_{c.m.} = 15°$ is due to "total

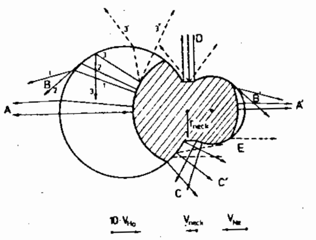

Fig. 9. The same situation as in Fig.7. Arrows mark the directions of emitted neutrons (see text). The c.m. velocities of projectile, target, and neck are proportional to the lengths of the corresponding horizontal arrows at the bottom of the figure.

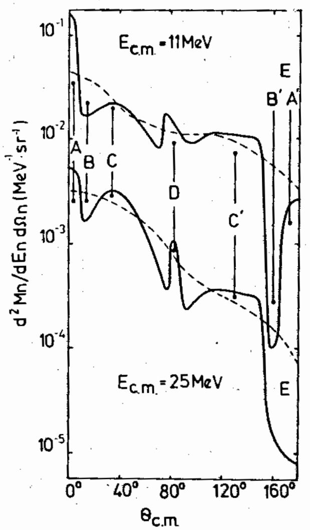

Fig. 10. Double-differential c.m. neutron multiplicities for the ^{20}Ne + ^{165}Ho, E_{lab}=220 MeV, L = 0 $\hbar$ system for 11 and 25 MeV neutron energies (full lines). The appearing structures are discussed in the text. The angle-averaged results are also shown (dashed lines).

reflection" of particles (cf. trajectory 3 in Fig. 9). A broader peak near $\theta_{c.m.}$ = 40° (C) corresponds to emission from the inner hemisphere of the Ne-nucleus. The sharp peak near $\theta_{c.m.}$ = 80° (D) is due to emission from the neck. Here, the combinatinn of the cylindrical geometry (instead of that of Fig. 1) and (18) produces a large spurious effect. The broad shoulder arround $\theta_{c.m.}$ = 130° (C') is the counterpart of C, i.e. stems from backward emission of the Ho-nucleus. The structures denoted by B', A' have the same origin like B,A, respectively. However, since the c.m. velocity of the Ne-nucleus is large, the backward focussing is not seen at all at 25 MeV due to transformation effects. In addition, at most backward angles (18) introduces an artificially large shadow effect (E), as can be seen from Fig. 9.

We emphasize that the differential multiplicities in the angular region C are much larger than in C', although the backward-emitting surface of the Ho-nucleus is larger than the forward-emitting surface of the Ne-nucleus. This is basically connected with the introduction of $\vec{V}(z,t)$ in (14): In the instantaneous rest system of the Ho-nucleus the mean velocity near the neck region (approaching

the Ho-nucleus with velocity $\dot{r}(t)/2$) and the velocity of the emitted particles have opposite directions, hence cos $\theta < 0$ in (14) and backward emission is suppressed (C'). The situation for forward emission from the Ne-nucleus (C) is similar in this respect. However, due to the substantial transformation effect for that nucleus, much smaller neutron energies (relative to the emitting surface) contribute to a given energy in the c.m. system. According to (14) the suppression effect is, consequently, less pronounced. Furthermore, since those neutrons escape with a higher probability, the peak denoted by C lies much above C' at 25 MeV (emission at the early stage - largest transformation effect) and slightly above C' in the 11 MeV case (emission at later instants - less pronounced transformation effect due to the decreased Ne-velocity).

To get rid of these spurious structures we average the calculated angular distributions over a certain angle interval $\Delta\theta$ (in the present calculations we use $\Delta\theta$= 60°) to obtain a monotonic behaviour that is expected if using (15) without the approximation (18), and the geometry of Fig. 1. To a certain extent this procedure may also simulate quantum mechanical distortion effects which should soften the classical-trajectory and classical-refraction descriptions used in our approach.

5.Comparison with Experimental Data

We now combine our PEP-model ($t < t_0$) with the HZ-model ($t_0 < t < \tau$) and compare the corresponding numerical results with recent experimental data.

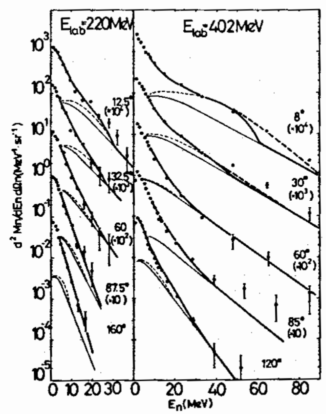

Fig. 11. Double-differential neutron multiplicities in coincidence with ER's from the ^{20}Ne + ^{165}Ho reaction at 220 and 402 MeV bombarding energies. The experimental points are from /20/. The thin full lines represent only the HZ-contributions. Adding the PEP-contributions for $t < t_0$ yields the thin dashed lines. The heavy full lines result if adding the evaporation part (the results of the corresponding fits of /20/ have been used). The heavy dashed lines denote the total contributions if a finite temperature is used in the PEP-stage (see text).

Fig. 11. concerns neutron emission from the ^{20}Ne + ^{165}Ho reaction at 11, and 20 MeV/A incident energy in coincidence with ER's. At both energies we get

a good agreement with the data without fitting any parameter. Formally, at highest neutron energies and most forward angles the agreement can be further improved by using a finite-temperature distribution at the PEP-stage. In the present case we have performed such a calculation for E_{lab}=402 MeV using $T_L^{PEP} = T_L^{HZ}(t_o)/2$, i.e. temperatures in the range 3 ÷ 4 MeV. It is, however, hard to justify such large values since the temperature due to absorption is less than 1 MeV for $t < t_o$. Rather the kink in the forward-angle spectra is related to our approximation of a sudden change of the emission mechanism at $t = t_o$. In reality, there should be a smooth transition, i.e. arround $t = t_o$ both emission of unscattered (PEP) or scattered particles should occur, while at instants much before and after the mechanism could be close to our extreme pictures.

It may be of interest to note that in our approach the relative weight of the HZ-contribution increases with bombarding energy, whereas both HZ- and PEP-contributions increase in absolute values. In the case illustrated in Fig. 11 the HZ-to-PEP multiplicity ratios are 6.1 at 11 MeV/A and 10.7 at 20 MeV/A. The absolute values are, however, about twice larger than the values extracted in /20/ from moving-source fits. We get M_n= 0.85 (2.84) total preequilibrium multiplicities compared to the fitted values M_n = 0.4 (1.5) at 11 (20) MeV/A. We relate this discrepancy to some overestimation of low-energy neutron emission since the use of Fermi gas level densities is no more justified for instants close to τ (when T_{HZ} has substantially decreased).

Due to the lack of a two-body friction in our trajectory calculations we presently cannot apply our model to incident energies much higher than 20 MeV/A. On the other hand, it is of interest to investigate our model predictions at comparably low energies since our arguments concerning the HZ seem to be more doubtful in this case. In Fig. 12 we compare our calculations with inclusive double-differential neutron cross sections for the reaction ^{20}Ne + ^{181}Ta at 9 MeV/A bombarding energy (4.2 MeV/A above the Coulomb barrier in the c.m. system). The agreement is still surprisingly good.

Fig. 13 illustrates the projectile-mass-number dependence of our model predictions at a fixed bombarding energy above the corresponding Coulomb barrier. We have chosen a comparably low energy since four data points are available in this case in the region of the most drastic increase of the calculated cross sections. The qualitative trends are the same at higher energies. We state that our results (PEP + HZ) agree reasonably with the data points. The slight underestimation for ^{12}C, ^{20}Ne projectiles (for the latter cf. also Fig.12)

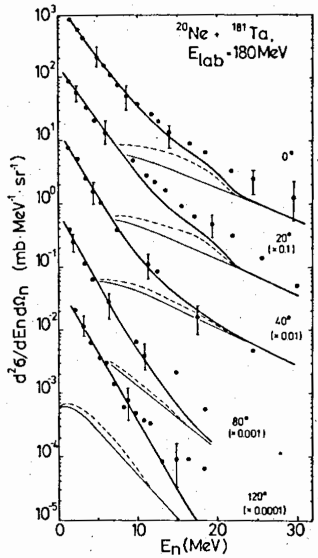

is partially connected with some contamination of the experimental results from evaporational neutrons. The present two-stage model predicts a stronger increase of the fast neutron cross section with the mass number of the projectile than the full PEP calculations which are also shown in Fig. 13. Also the absolute values are much larger except for very light projectiles.

Fig. 12. Double-differential cross sections for inclusive neutron emission from the ^{20}Ne + ^{181}Ta, E_{lab} = 180 MeV reaction /49/. The curves have the same meaning as in Fig.11.

Due to certain difficulties arising even in our modification /39/ of the Bertsch model for extremely asymmetric systems, we could not extend the calculations down to ^{4}He-projectiles. Note that the relative weight of HZ-emission is also an increasing function of the projectile mass (77.5% for ^{12}C, 90.5% for ^{181}Ta).

We conclude that in our approach PEP-emission is favoured in very asymmetric systems and at comparably low incident energies while in the opposite cases the HZ-emission dominates.

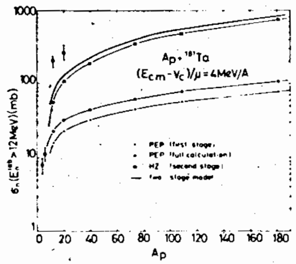

Fig. 13. Projectile-mass dependence of the inclusive cross sections for fast neutron emission (E_n > 12 MeV in the laboratory system) for reactions with a ^{181}Ta target at bombarding energies of 4 MeV/A above the Coulomb barrier in the c.m. system. The predictions of our two-stage model are compared to a few experimental points taken from /49/ as well as to a full PEP calculations.

Exceptions are the most forward angles where the relative PEP-contributions seem even to increase with increasing incident energy (cf. Fig. 11).

Finally, we speculate about higher bombarding energies. If it is increased, the contact time during which our model dynamically describes something like a mid-rapidity, high-temperature (T_h)

source certainly decreases. For more and more impact parameters (starting from more peripheral collisions) it may become smaller than τ. Then, at scission, the smaller projectile is fully equilibrated while the target is not (the front has not yet reached the outer surface) but the temperatures in the HZ region of the target and in the projectile (T_P) are the same and still quite large. Subsequently, the target equilibrates isolated from the projectile and consequently its final temperature T_T is the smallest: $T_T < T_P < T_h$. This is exactly the situation obtained in /50/ with respect to inclusive proton emission for the $^{12}C + ^{58}Ni$ reaction. In /50/ values of $T_T/T_P/T_h$ of 4.2/5.5/7.7 MeV and 6.7/10.2/19.2 MeV have been fitted at 25 and 84 MeV/A, respectively.

6. Conclusions

Starting from recent results of the VUU and ETDHF approaches and some experimental indications of the existence of a spatially localized, rapidly expanding HZ, we have proposed a parameter-free phenomenological two-stage model for fast nucleon emission combining PEP-emission at the early stage and emission from a highly anisotropic HZ at the later stage of the equilibration process. The agreement with data on neutron emission in coincidence with ER's as well as with inclusive neutron data is remarkably good - even at lower incident energies where our assumptions concerning the HZ-stage are less founded.

We believe that our HZ-model can be viewed as a dynamical description of the mid-rapidity high-temperature source seen in VUU-calculations and used as a standard parametrization to analyze fast--particle data since at $t \gtrsim t_0$

i) the HZ involves $\bar{v}(z,t)$ -values ranging from projectile - to target-like velocities above the Coulomb barrier (hence, the "effective" source velocity appears to be intermediate),

ii) the HZ-temperatures are close to the values obtained from moving-source fits, and

iii) the "effective" particle number in the HZ is roughly twice the mass number of the projectile (cf. Figs. 7,9).

Qualitative extrapolations to higher bombarding energies lead to a hierarchy of temperatures and velocities as obtained in a recent three-source parametrization.

We emphasize that in our model the excitation energy is initially nearly equally shared by projectile and target as it has been observed in experiment /51/. In the subsequent evolution the system smoothly approaches a deposition of the excitation energy proportional to the mass numbers of the colliding nuclei.

Our assumptions on the time-evolution of the HZ are at best lowest-order approximations and should be further improved, especially if corresponding VUU- (or realistic ETDHF-) calculations would exhibit substantially different temperature- and velocity fields. For a further proof of the present model, more detailed information from those approaches about the early stage of the collision is highly requested. Furthermore, a two-body friction term should be included in the trajectory calculations, although, at not too high energies, it may turn out to be not essential in the time interval of interest ($t < \tau$).

Part of the results contained in the present work has been obtained in /52/. A brief description of the basic ideas as well as some preliminary results have been published in /53/.

Acknowledgement: The authors are very grateful to R.Reif for his permanent interest in the present work, many critical remarks and stimulating discussions.

References

1. Gelbke C.K. Proc. Workshop on Coincident Particle Emission from Continuum States, Bad Honnef, June 1984, Machner H., Jahn P. (eds.), p. 2030, World Scientific 1984;
Hilscher P. et al.: ibid., p. 268.
2. Weiner R., Weström M. Nucl.Phys., 1977, A286, p. 282.
3. Gottschalk P.A., Weström M. Nucl.Phys., 1979, A314, p.232.
4. Garpman S.I.A., Sperber D., Zielinska-Pfabe M. Phys.Lett., 1980, 90B, p. 53.
5. Blann M. Phys.Rev., 1981, C23, p. 205.
6. Blann M. Phys.Rev., 1985, C31, p. 1245.
7. Yoshida S. Z.Phys., 1982, A308, p. 133.
8. Nijta K. Z.Phys., 1984, A316, p.309.
9. Machner H. et al. Phys.Rev., 1985, C31, p. 443.
10. Awes T.C. et al. Phys.Rev., 1982, C25, p. 236.
11. Bondorf J.P. et al. Nucl.Phys., 1980, A333, p. 285.
12. Sebille F., Remaud B. Z.Phys., 1983, A310, p. 99.
13. Tricoire H. Z.Phys., 1983, A312, p. 221.
14. Davies K.T.R. et al. Ann.Phys. (N.Y.), 1984, 196, p. 68.
15. Leray S. et al. Z.Phys., 1985, A320, p. 383.
16. Cassing W. Nucl.Phys., 1985, A438, p. 253.
17. Umar A.S. et al. Phys.Rev., 1984, C30, p. 1934.

18. Devi K.R.S. et al. Phys.Rev., 1981, C24, p. 2521.
19. Dhar A.K. et al. Phys.Rev., 1982, C25, p. 1432.
20. Holub E. et al. Phys.Rev., 1983, C28, p. 252.
21. Jakobsson B. et al. Phys.Lett., 1981, 102B, p. 121.
22. Oskarsson A. Lund University Report 8303, 1983.
23. Tsang M.B. et al. Phys.Lett., 1984, 148B, p. 265.
24. Tsang M.B. et al. Phys.Rev.Lett., 1984, 52, p. 1967.
25. Kruse H. et al. Phys.Rev., 1985, C31, p. 1770.
26. Aichelin J., Stöcker H. Proc. Int. Workshop on Gross Properties of Nuclei and Nuclear Excitations, Hirschegg, Austria, January 1985, Feldmeier H. (ed.), p. 210.
27. Aichelin J., Bertsch G. Phys.Rev., 1985, C31, p. 1730.
28. Aichelin J., Stöcker H. to be published.
29. Köhler H.S. Physica Scripta, 1982, 26, p. 51.
30. Köhler H.S. Nucl.Phys., 1984, A417, p. 541.
31. Köhler H.S. Nucl. Phys., 1985, A438, p. 564.
32. Köhler H.S. Nucl.Phys., 1985, A440, p. 165.
33. Bonche P., Koonin S., Negele J.W. Phys.Rev., 1976, C13, p. 1226.
34. Danielewicz P. Ann.Phys. (N.Y.), 1984, 152, p. 239; p. 305.
35. Karvinen A.O.T., De J.N., Jakobsson B. Nucl.Phys., 1981, A367, p. 122.
36. Biedermann M., Mädler P. In preparation.
37. Bertsch G.F. Preprint MSUCL-385, 1982.
38. Ko C.M., Bertsch G.F., Cha P. Phys.Lett., 1978, 77B, p. 174.
39. Biedermann M., Mädler P., Reif R. JINR Communication E7-84-415, 1984.
40. Sinha B. Phys.Rev.Lett., 1983, 50, p. 91.
41. Toki H., Stöcker H. Phys.Lett., 1985, 152B, p. 326.
42. Carruthers P. Preprint LA-UR-85-280, 1985.
43. Chiang H.C., Hüfner J. Nucl.Phys., 1980, A349, p. 466.
44. Mädler P., Reif R. Nucl.Phys., 1982, A373, p. 27.
45. Chitwood C.B. et al. Phys.Rev.Lett., 1985, 54, p. 302.
46. Lynch W.G. et al. Phys.Rev.Lett., 1983, 51, p. 1850; 1984, 52, p. 2302.
47. Bernstein M.A. et al. Phys. Rev.Lett., 1985, 54, p. 402.
48. Mädler P. Z.Phys., 1984, A318, p. 87.
49. Kozulin E.M. et al. Preprint JINR P7-85-31, 1985.
50. Glasow R. et al. p. 299 of ref./1/.
51. Vandenbosch R. et al. Phys.Rev.Lett., 1984, 52, p. 1964.
52. Biedermann M. Diploma thesis, Technical University Dresden, 1984.
53. Biedermann M., Mädler P.: p. 218 of ref./26/.

Received by Publishing Department
on July 26, 1985.